

Dam breaking seiches

N. J. Balmforth¹, J. von Hardenberg² and R. J. Zammett³

¹Depts. of Mathematics and Earth & Ocean Science, UBC, Vancouver, BC

²Institute of Atmospheric Sciences and Climate, CNR, Lecce, Italy

³Department of Mathematics, University of Oxford, UK

(Received 26 March 2008)

Experimental and theoretical models are used to explore the break of a moraine dam by catastrophic erosional incision initiated by overtopping with a displacement wave. The experiments are conducted in a rectangular tank with an erodible barrier made from sand and grit. Theory combines shallow-water hydrodynamics with an empirical model of erosion. The models confirm that dams can be broken by a catastrophic incision. However, the displacement wave does not break the dam in its first passage, but excites a long-lived seiche that repeatedly washes over the dam, which initially remains intact. The cumulative erosion of the downstream face by the overtopping seiches eventually allows an incipient channel to form, and catastrophic incision follows. Estimates are presented of the strength of the disturbance required to break the dam and the maximum discharge that can be achieved during the breach.

1. Introduction

Many moraine-dammed lakes have been left behind by the retreat of glaciers in mountainous regions worldwide due to the warming of the climate. These reservoirs constitute natural hazards should the dam break suddenly. Indeed, geological evidence points to a number of recent failures of moraine dams, which released much of the dammed water and created dangerous floods downstream (Clague & Evans 2000). One of the principal causes of moraine dam failure is claimed to be catastrophic erosional incision, as initiated either by a gradual overfilling during unusual weather conditions, or by a large wave suddenly overtopping the dam (see Clague & Evans 2000).

The moraine which dammed Lake Tempanos in Argentina, for instance, appears to have failed in the 1940s due to meltwater accompanying a 350 m retreat of the glacier (Rabassa, Rubulis & Suarez 1979). On the other hand, large destructive waves can be generated by ice or rock falls, which are likely given that moraine-dammed lakes are often located in steep alpine valleys, or beneath the unstable toe of the retreating glacier. For example, a rock avalanche into the glacial lake Safuna Alta created a displacement wave over 100 m high (Hubbard *et al.* 2005), and although this particular example failed to break the dam, it was responsible for significant erosion. Displacement waves are more typically thought to be tens of meters high (Costa & Schuster 1988).

The key to the catastrophic incision mechanism is that the overflow or overtopping wave notches an incipient channel at the top of the dam. The increased flow through that opening erodes and deepens the channel still further, which accelerates the outflow and the erosion, and a runaway incision ensues. Typically, the lakes are kilometers long, hundreds of meters wide, and have depths of tens of meters; millions of cubic meters of water are released by the catastrophic incision, with peak discharges of up to $10^3 - 10^4$

$\text{m}^3 \text{sec}^{-1}$ (Clague & Evans 2000). Artificial earthen dams are known to suffer catastrophic erosional incision when the adjoining reservoir is overfilled, and various theoretical and experimental models of the process have been constructed (*e.g.* Walder & O’Connor 1997; Coleman et al. 2002; Cao et al. 2004). By contrast, the failure of a moraine-dammed lake has never been directly witnessed, and triggering incision with a large overtopping wave has not previously been modelled in any detail.

Our main objectives in the current study are to determine under what conditions a wave can initiate runaway incision and break a dam. We also examine properties of the resulting flood, such as the maximum discharge and the duration of the dambreak. In principle, these results bear on the important geological issues of outburst probability and hazard control and mitigation (McKillop & Clague 2006, 2007). Our approach is on the idealized side and combines experimental and theoretical studies.

The experiments are conducted in a “scaled down” laboratory setting, in the sense that the rough geometrical aspects of the lake-moraine system are reduced proportionately. However, we cannot accurately scale down either the material properties of the erodible dam, or the dynamics of the turbulent water flow. Part of the difficulty is the lack of detailed information on the material properties of glacial moraines (but see Clarke 1987 and Clague & Evans 2000). To reproduce the turbulent dynamics, we would have to resort to a bigger apparatus. Instead, we opt for a simpler, more qualitative approach, which can at least make firmer contact with the accompanying theory.

The theory couples shallow-water equations for the fluid flow with an empirical erosion law that determines the height of the dam. The model is two-dimensional, describing the evolution in time of the fluid depth, velocity and bed elevation along the tank length; a short discussion of three-dimensional dynamics is reported by Balmforth, von Hardenberg, Provenzale & Zammett 2008. Finally, guided by both the theory and experiments, we outline a simpler model of the dambreak dynamics that can be used to gauge the effect of the various physical parameters of the problem and which can be extended to explore the motivating geophysical application.

2. Experiments

2.1. Setup

The setup for our experiments is shown in figure 1, and consists of a rectangular glass tank with length 125 cm and depth 30 cm. The width of the tank was 20 cm, but by inserting a second panel it could be reduced to 5 cm. The downstream end of the tank was open to allow water and sediment to drain from the tank. The dams were built in a Gaussian shape using an appropriately shaped stencil, with heights about 10 cm and lengths of about 40 cm (4 standard deviations of the Gaussian). They were positioned to leave a metre-long reservoir that was filled with water up to a depth close to the top of the dam.

The water was then left to seep through the dam to make sure that it could withstand the hydraulic water pressure. A wave was initiated in the reservoir by sweeping water towards the dam using a paddle. A video camera captured the resulting action. From the video images we extracted profiles of the dam and water depth; by floating tracer particles on the water surface we estimated flow speeds.

Glacial moraines are poorly sorted and loosely consolidated sediments with particle sizes ranging from fine clays to large boulders. Clarke (1987) notes that moraine sediments can have a bimodal particle size distribution. Based on these observations, we used a variety of experimental materials to construct the dams: three types of sand and

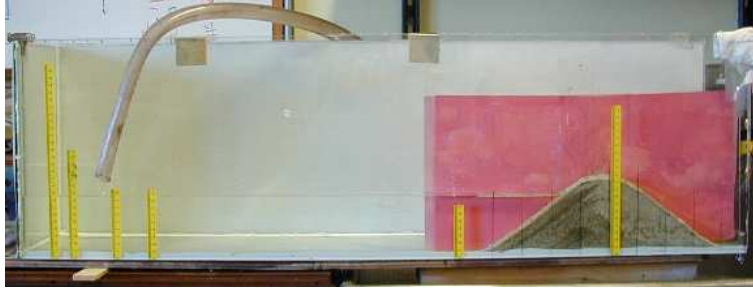


FIGURE 1. The experimental setup.

Sediment	ρ (10^3 kg m^{-3})	Porosity	Modal particle size (μm)	Angle of repose
Medium Sand	2.34	0.38	310	36°
Coarse Sand	2.34	0.35	950	36°
Grit	2.42	0.42	1150	34°
Fine sand/grit mix	2.38	0.32	250 & 1150	36°
Medium sand/grit mix	2.36	0.37	310 & 1150	38°

TABLE 1. Properties (when dry) of the individual sediments and mixes that were used to build the dams. Density was calculated from the weight of a given sediment volume once the sediment porosity was determined. Sediment porosity was measured by measuring how much water was absorbed by a given volume of sediment. Modal particle size was estimated from distributions obtained by laser diffraction. The angles of repose are averages over measurements of tilting a pile of sediment or creating a conical pile of the sediment.

a coarser grit. The sands had relatively wide particle size distributions, but different mean diameters (and are therefore referred to as “fine”, “medium” and “coarse”), whereas the grit consisted of larger particles of roughly equal size. To make sediments with bimodal particle size distributions, we mixed the grit with one of the sands in roughly equal proportions. The materials, their mean particle sizes and some other properties are listed in table 1.

Only some of the materials listed in table 1 were found to be suitable for dam construction: dams built from the medium sand were not sufficiently strong to support themselves against the water pressure, and collapsed before a wave was even initiated (the fine sand by itself was even worse, and so this material was rejected immediately and used only in the mixtures). The grit made a very porous obstruction, and water drained quickly through, leading to waterlogged structures that became unstable as the downstream face mobilized and slumped. It was also hard to incise a channel in the grit dams because the overtopping water often seeped into the dam rather than eroding it.

Overall, the coarse sand and the two sand/gravel mixtures proved to be the best materials, in terms of providing a dam that was both stable and erodible by overtopping waves. We speculate that this is because all three materials contained roughly equal amounts of relatively large and small particles: the larger particles contributed to dam stability, whilst the smaller particles blocked the seepage through the structure and allowed greater erodibility. This suggests that the composition of glacial moraines might

be key in setting the stage for catastrophic erosional incision and may explain why the phenomenon is not seen in other natural dams, such as those formed by landslides.

2.2. Dambreak phenomenology

By varying both the amplitude of the initial disturbances in the reservoir and the material used to build the dam, we were able to initiate runaway incisions. The pattern of evolution, however, took an unexpected turn. Initially, the disturbance generated a large wave that overtopped the dam. During its passage, the wave eroded a significant fraction of the downstream face of the dam. However, in none of the experiments was that wave able to create an incipient channel through which a catastrophic incision could ensue (overly strong waves caused a mechanical failure of the whole structure).

Instead, a large fraction of the wave was reflected back into the reservoir and propagated to the back wall of the tank where it was again reflected back towards the dam. A second overtopping then followed, together with a second reflection from the dam. Fairly quickly, the reflecting wave settled into a regular seiche of the reservoir, with periodic overtoppings at the dam during each cycle. Each overtopping contributed to the erosion of the downstream face of the dam, plus some removal of material from its peak. When conditions were favourable, the cumulative effect was to cut an incipient channel, and a catastrophic incision followed that emptied the majority of the reservoir within a minute. The number of waves needed to initiate runaway incision varied between the experiments, ranging from as few 5 waves, to more than 20.

Some images of dam breaks for the narrow (5 cm) and wide (20 cm) tank are shown in figures 2 and 3, respectively. The figures also display snapshots of the evolving profile of the dams, together with time series showing the dam's maximum height and position, the water depth in the reservoir and the water depth at the dam maximum. The profiles illustrate how the fluid flow primarily erodes the downstream flank of the dam. Towards the end of the experiments, the erosion slows as the reservoir level declines, leaving intact a shallow, wedge-shaped structure whose upstream edge is a relic of the original dam. A weak outflow washes over the broken dam, but is sufficiently gentle to leave the ruin in place.

Catastrophic erosional incision was successful in breaking the dams only provided the initial disturbance was sufficiently strong; a lower-amplitude disturbance still excited a seiche together with some wave overtoppings, but these eventually subsided to leave the obstruction intact. An example of an unsuccessful dam break experiment in which catastrophic incision did not occur is shown in figure 4. In view of the simple method used to generate the initial disturbance, we did not attempt a detailed experimental study of the threshold. Nevertheless, it was possible to extract estimates of the initial wave amplitudes from the video recordings. For the coarse sand dams shown in figures 2 and 3, the critical wave amplitude, as measured by the elevation of the water surface, was about ten percent of the reservoir depth.

The threshold results because the initial wave must be sufficiently strong that the seiche can repeatedly spill over the dam and cut an incipient channel, whilst dissipation saps its strength and drainage lowers the reservoir level. When the seiche did not spill over the dam (either because overtopping had stopped or because the amplitude of the initial disturbance was not large enough), the decay of its amplitude took an exponential form and could be reproduced by Keulegan's (1959) viscous boundary layer model. In other words, dissipation inside Stokes layers adjacent to the walls was primarily responsible for damping the seiche. On the other hand, the decay was stronger when the seiche spilled over the dam, suggesting that either transmission of the wave energy across that barrier or turbulent drag also play a role.

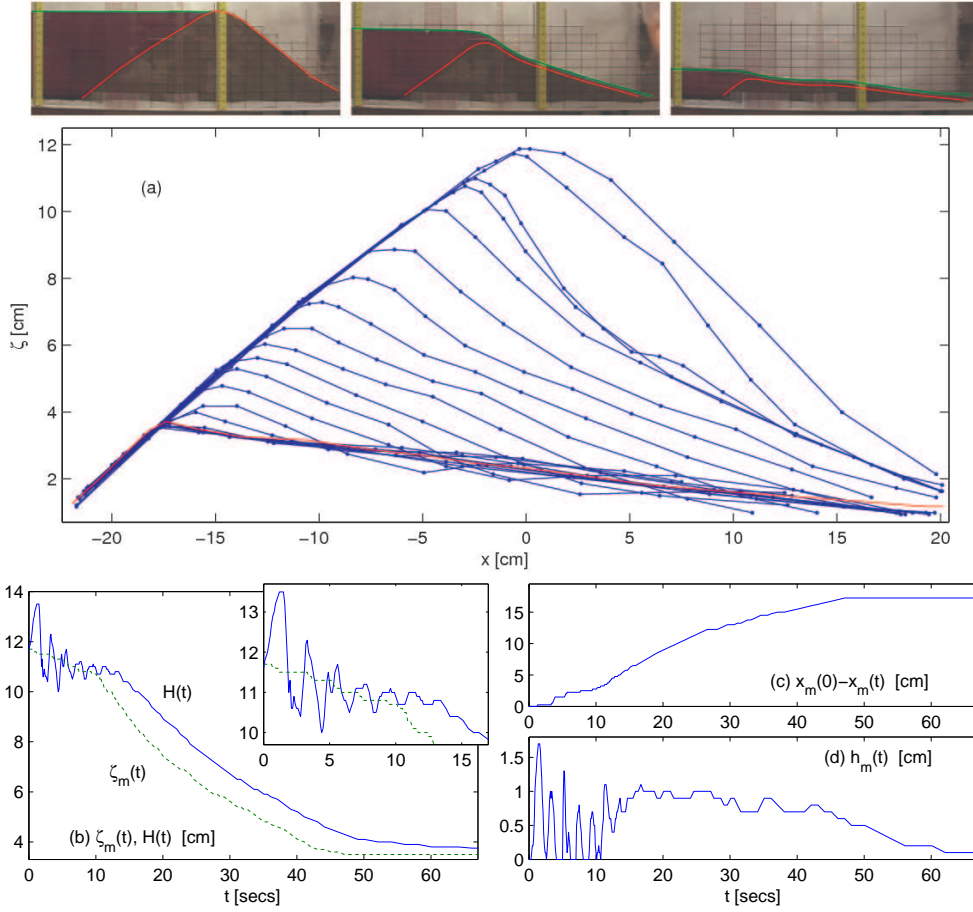


FIGURE 2. A successful dam break in the narrow tank. Shown are three photographs (before and during the dambreak) plus (in panel (a)) a sequence of curves plotting the dam height every 3 seconds for 60 seconds. The wedge-shaped final state to which the eroded dam converges is also plotted. The lower panels show (b) the reservoir depth, $H(t)$, and maximum dam height, $\zeta_m(t)$, (c) the shift in the position of the dam's maximum, $x_m(0) - x_m(t)$, and (d) the water depth at that maximum, $h_m(t)$.

Figure 5 shows some further details of the flow dynamics during the catastrophic incision in the experiment of figure 3. The picture displays the dam height, ζ , water depth, h , and speed, u , as one moves through the breach in the dam, obtained by following the position of a tracer on the water surface. From these measurements, the flux, hu , and “Bernoulli potential”, $B = g(h + \zeta) + u^2/2$, are calculated. The shallow-water theory described in the next section implies that when the flow is steady and drag is not important, the potential and the water flux should be constant across the breach. There is indeed some suggestion that the water flux is roughly constant moving with the particle, but the data is not very conclusive because the estimates of speed u are not very precise. Overall, B decreases by about fifty percent as tracer the particles travel through the breach, suggesting that turbulent drag again plays a role.

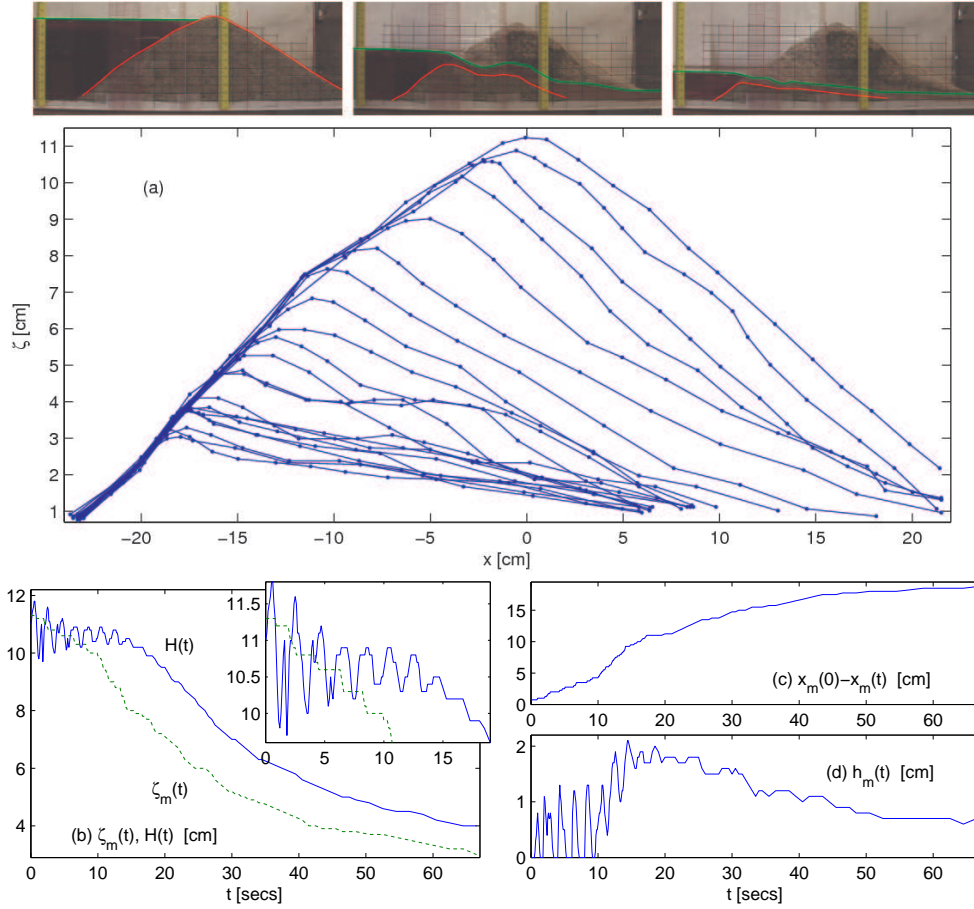


FIGURE 3. A successful dam break in the wide tank. Shown are three photographs (beginning and during) plus (in panel (a)) a sequence of curves plotting the dam height every 3 seconds for 63 seconds. The lower panels show (b) the reservoir depth, $H(t)$, and maximum dam height, $\zeta_m(t)$, (c) the shift in the position of the dam's maximum, $x_m(0) - x_m(t)$, and (d) the water depth at that maximum, $h_m(t)$.

2.3. Channelization and effect of tank width

An important difference between the dam breaks in figures 2 and 3 is that the dam in the narrow tank erodes in an almost two-dimensional fashion while in the wide tank the obstruction is channelized by the overtopping waves. This creates a breach whose width is some fraction of that of the dam, as shown by the photograph inset into figure 6. Although we did not systematically study the width of such incisions, we found large differences between experiments with the same dam materials and similar initial conditions. The two experiments in the wide tank with dams constructed of coarse sand presented in the main panel of figure 6, for example, formed breaches whose maximum widths were about 6 cm and 10 cm (one third and one half of the dam width); in figure 3, the largely uneroded parts of the initial dam are visible in the background.

Figure 6 also plots reservoir depth against time for a number of experiments with dams made from coarse sand alone, or the mix of medium sand and grit. The coarse sand dams erode significantly faster, illustrating the important effect of dam composition on the incision. More surprisingly, there is little difference between experiments with the same

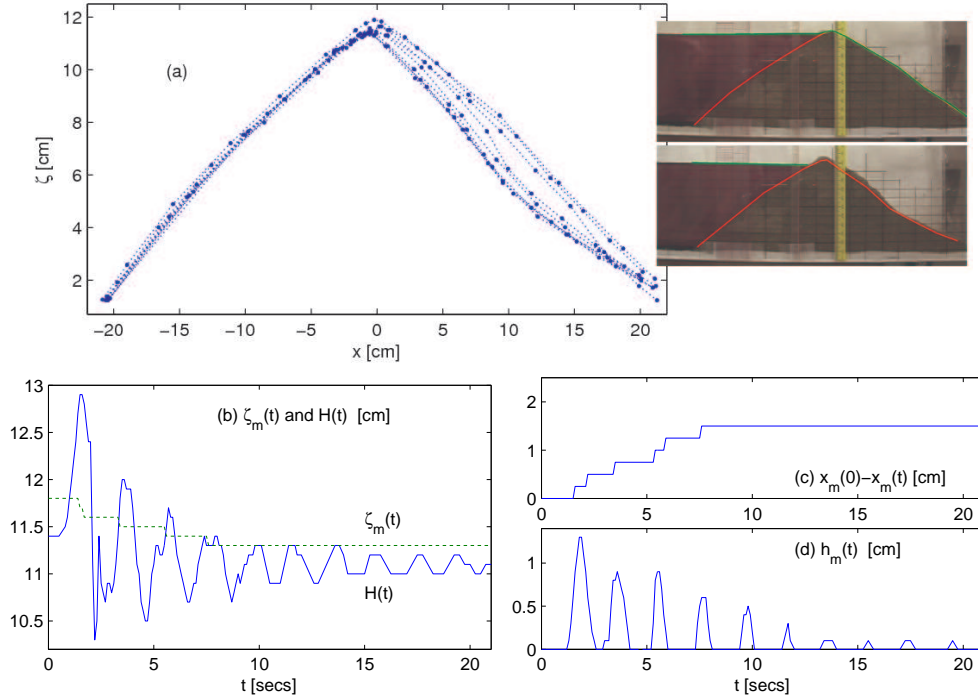


FIGURE 4. An unsuccessful dam break in the narrow tank. Shown are two photographs (before and after), plus (in panel (a)) a sequence of curves plotting the dam height every 2 seconds for 16 seconds. The measurement errors can be seen on the left-hand side of the dam, where very little erosion or sediment movement actually takes place. The lower panels show (b) the reservoir depth, $H(t)$, and maximum dam height, $\zeta_m(t)$, (c) the shift in the position of the dam's maximum, $x_m(0) - x_m(t)$, and (d) the water depth at that maximum, $h_m(t)$.

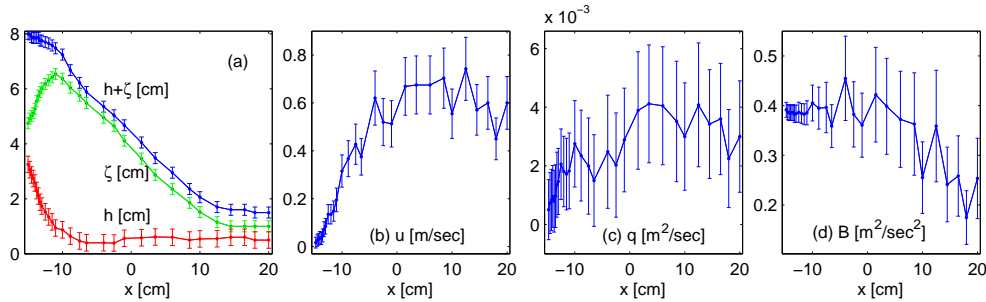


FIGURE 5. Plots of (a) the free surface, $h + \zeta$, maximum dam height, ζ , and water depth, h , (b) speed, u , (c) flux, $q = hu$, and (d) $B = g(h + \zeta) + u^2/2$ against position through the breach (with the origin located at the original maximum elevation of the dam), for a sample tracer particle during the experiment of figure 2. The error bars reflect errors in the measurement of position as extracted from video recordings.

material but with the two different tank widths. despite the occurrence of channelization in the wide cases. Moreover, the wide tank experiments show little variation between one another even though the channelized breaches could have quite different widths.

In the wide tank, there were occasional avalanches of sediment from the sides of the incised channel as it deepened and the sides steepened. Upstream migrating bedforms, travelling at speeds of a few centimeters per second, also appeared once the channel

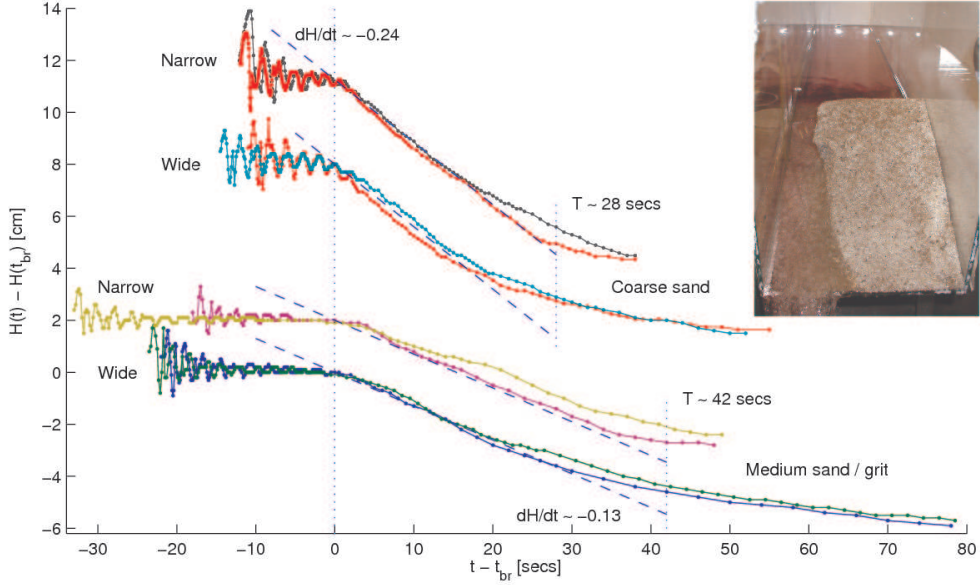


FIGURE 6. Plots of reservoir depth against time for dams constructed of coarse sand, and the medium sand/grit mix, both in the wide and narrow tank. For each sediment, two experiments are displayed. The origin of time is shifted to the estimated moment of dam break, and the change in depth from that moment is plotted. The curves for the different pairs of experiments are offset from one another for clarity, and lines showing characteristic slopes for dH/dt are also added. The time for the incision to occur is indicated (and denoted T). The inset shows a photograph of an incised dam of coarse sand in the wide tank (an instant in the experiment of figure 3).

was established (the undulation of the bed in the second photograph of figure 3 is one such example). Both bedforms and channelization can be interpreted in terms of linear instabilities predicted in uniform streams (Balmforth *et al.* 2008).

3. A shallow water model

3.1. Governing equations

To model the fluid dynamics, we use the Saint-Venant equations: The flow is described by the local velocity, $u(x, t)$, and depth, $h(x, t)$, which satisfy

$$h_t + (hu)_x = 0, \quad (3.1)$$

and

$$u_t + uu_x = -g(\zeta + h)_x - \Gamma u + (\nu_T u_x)_x, \quad (3.2)$$

where the subscripts x and t denote partial derivatives, the surface $z = \zeta(x, t)$ represents the underlying erodible bed, Γ is a drag coefficient (with units of sec^{-1}) that measures the stress exerted on the fluid by the bed, g is gravitational acceleration, and ν_T is a (turbulent or otherwise) viscosity with units of m^2/sec that is assumed to be constant in this analysis. The geometry is shown in figure 7. The erodible material is piled up to form a dam on top of the x -axis, which is taken to be immobile, so $\zeta > 0$.

For the bottom drag, we take

$$\Gamma = h^{-1}(C_f |u| + \Lambda),$$

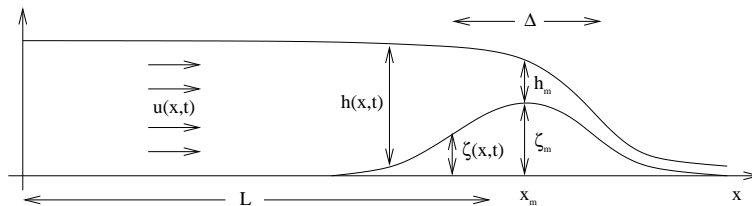


FIGURE 7. A sketch of the shallow-water configuration.

so that C_f is a dimensionless turbulent, Chézy-like coefficient and Λ a simple friction factor (with units of m/sec). We include both to account for the leading-order effect of turbulent stresses in geophysical settings, and laminar viscous drag which is important in the laboratory.

To model how material is lifted off the dam and transported downstream, we assume that the bed is eroded at a rate that depends on the stress exerted by the fluid, which is given by u^2 . This leads us to an Exner equation for the bed elevation,

$$\zeta_t = -WE(u^2), \quad (3.3)$$

where W is a characteristic erosion parameter and $E(X)$ is a suitable function modelling the precise dependence of erosion on stress. We take

$$E(u^2) = \begin{cases} 0, & u^2 < U_*^2, \\ (u^2 - U_*^2)^\alpha, & u^2 \geq U_*^2, \end{cases} \quad (3.4)$$

where U_* denotes a threshold speed below which erosion does not take place, and α is an empirically-determined parameter that we fix equal to $3/2$ in the following (*cf.* Parker 2006). This formulation for erosion was used by Taki & Parker (2004) and Cao *et al.* (2004), amongst others.

After being suspended in the fluid for a time, where it is advected and mixed by turbulence, the eroded material will ultimately sediment under gravity and fall back onto the bed. Such effects can be incorporated into the model by including an additional variable representing the concentration of suspended load (see Balmforth *et al.* 2008). Nevertheless, the dam break dynamics are not particularly sensitive to deposition since it plays little role at the crest of the dam which determines much of the overall behaviour. In the interest of brevity, we have therefore omitted this generalization of the model. Note also that the formulation above does not take into account the sources of mass and momentum in the fluid equations due to erosion and deposition. This is a simplifying approximation that is known to be inaccurate in some related contexts (Cao *et al.* 2004). Elsewhere (Balmforth *et al.* 2008), we found that including the feedback of the sediment on the water flow had no qualitative effect.

3.2. Dimensionless form

We place the equations in a dimensionless form as follows. Let Z_0 denote the initial height of the dam and Δ denote a measure of its width. Then, we set

$$x = \Delta \tilde{x}, \quad t = \frac{\Delta}{\sqrt{gZ_0}} \tilde{t}, \quad u = \sqrt{gZ_0} \tilde{u}, \quad (h, \zeta) = Z_0(\tilde{h}, \tilde{\zeta}), \quad (3.5)$$

which, after dropping the tilde, leaves the dimensionless system,

$$h_t + (hu)_x = 0, \quad (3.6)$$

$$u_t + uu_x = -h_x - \zeta_x - (c_f|u| + \lambda)\frac{u}{h} + \nu u_{xx}, \quad (3.7)$$

$$\zeta_t = -\epsilon E(u^2), \quad (3.8)$$

where

$$\epsilon = \frac{W\Delta}{Z_0}(gZ_0)^{\alpha-1/2}, \quad (3.9)$$

$$E(u^2) = \begin{cases} 0, & u^2 < u_*^2 \\ (u^2 - u_*^2)^\alpha, & u^2 \geq u_*^2 \end{cases}, \quad u_* = U_*/\sqrt{gZ_0}, \quad (3.10)$$

$$\nu = \frac{\nu_T}{\Delta\sqrt{gZ_0}}, \quad c_f = \frac{\Delta C_f}{Z_0} \quad \text{and} \quad \lambda = \frac{\Lambda\Delta}{Z_0\sqrt{gZ_0}}. \quad (3.11)$$

We solve the system (3.6)–(3.8) numerically in the domain, $0 < x < 2\ell$, with a suitable initial condition. We position the maximum of the initial dam at $x = \ell$, with the reservoir occupying the region $0 < x < \ell$ (so ℓ is the lake length in units of dam width: $\ell = L/\Delta$). Specifically, we adopt

$$\zeta(x, t = 0) = e^{-\frac{1}{2}(\ell-x)^2}, \quad (3.12)$$

$$h(x, t = 0) = h_{eq}(x) + A_0 \sin(2\pi x/\ell), \quad h_{eq}(x) = \begin{cases} h_0 - \zeta(x) & h_0 > \zeta \text{ and } x < \ell, \\ 0 & \text{otherwise.} \end{cases} \quad (3.13)$$

where h_0 and A_0 are parameters. That is, $\zeta(x, 0)$ and $h_{eq}(x)$ parameterize an undisturbed lake configuration on which we launch a wave with amplitude A_0 . The undisturbed lake level lies at a dimensionless distance of $1 - h_0$ below the top of the dam.

For boundary conditions, we take $u = h_x = 0$ at $x = 0$ and impose “open” flow conditions, $u_x = h_x = 0$, at $x = 2\ell$. Equations (3.6)–(3.8) are integrated numerically with a Leapfrog-Adams-Moulton predictor-corrector scheme in time and a second-order-accurate finite difference scheme in space, using a staggered grid. A Flux Corrected Transport scheme (Boris & Book 1975, Zalesak 1979) is used for the positive definite variable, h . We also “regularize” the bottom friction terms in equation (3.7) by replacing the denominator by $\sqrt{h^2 + 10^{-8}}$.

3.3. Numerical results

Figure 8 presents two sample numerical solutions with different initial wave amplitudes. It displays the evolution of the water surface, $h(x, t) + \zeta(x, t)$, in space and time, as well as time series of the reservoir depth and dam height, and a series of snapshots of the dam profile. In each case, the initial disturbance generates waves that subside into a regular seiche after a short time. The spilling of the seiche over the dam generates pulses in discharge that sequentially lower the barrier and make the location of the dam’s maximum recede upstream. The higher amplitude initial wave ultimately breaks the dam after about seven periods of the seiche, whereas the weaker disturbance leaves the obstruction in place (in this case, the final decay of the seiche matches the exponential form expected for the linear normal mode, as shown in figure 8c).

More details of the breaching process are displayed in figure 9. During the runaway incision the flux $q = hu$ is roughly constant in space, as observed in the experiments (see section 2). The corresponding (dimensionless) Bernoulli potential, $\mathcal{B} = u^2/2 + h + \zeta$, varies quite sharply with x during this phase, reflecting how the dissipative and unsteady terms in the shallow-water computations are not negligible. This is one point of disagreement between the shallow-water theory and the reduced model described shortly.

The theoretical dambreak threshold on the (ϵ, A_0) -plane is presented in figure 10. Also displayed are the number of waves that are needed to initiate the dambreak. The details of this plot depend on the various other parameters in the problem and the form

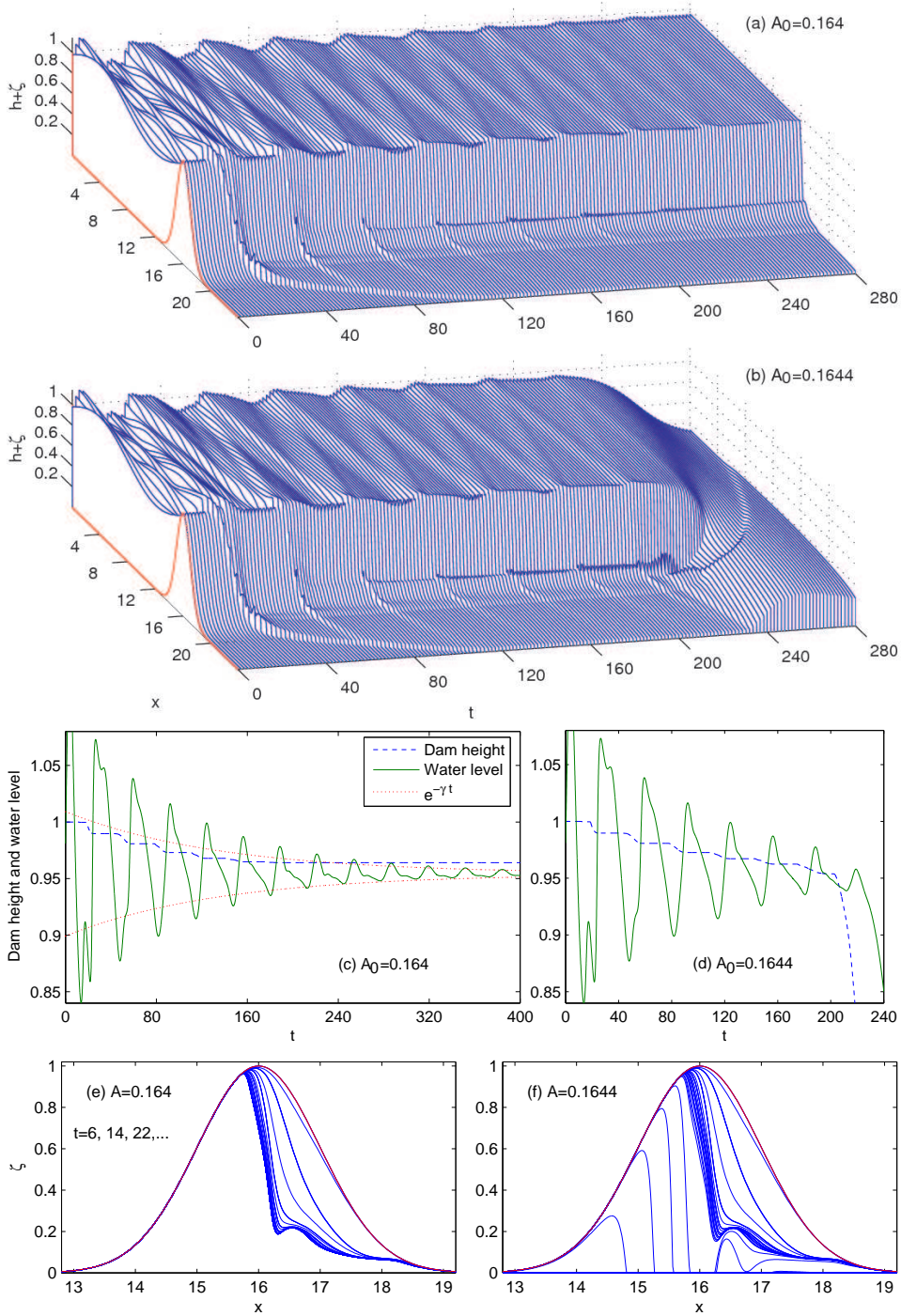


FIGURE 8. Numerical solutions of the shallow-water model near threshold. The initial waves have amplitude of $A_0 = 0.164$ and 0.1644 . The elevation of the water surface, $h(x, t) + \zeta(x, t)$, is shown (panels (a), (b)) as a surface over the (t, x) -plane. Other panels show the dam height and the water level in the upstream basin as a function of time (panels (c), (d)) and the evolution of the dam profile (panels (e), (f)). The parameter settings: $\epsilon = 0.25$, $u_* = 0.1$, $\nu = 0.04$, $c_f = 0.0125$, $\ell = 16$, $\alpha = 3/2$, $h_0 = 0.98$ and $\lambda = 0.0125$, and there are 2048 gridpoints in x . In panel (c), the expected exponential decay (with exponent $\gamma \approx 0.0074$) of the linear seiche is also shown.

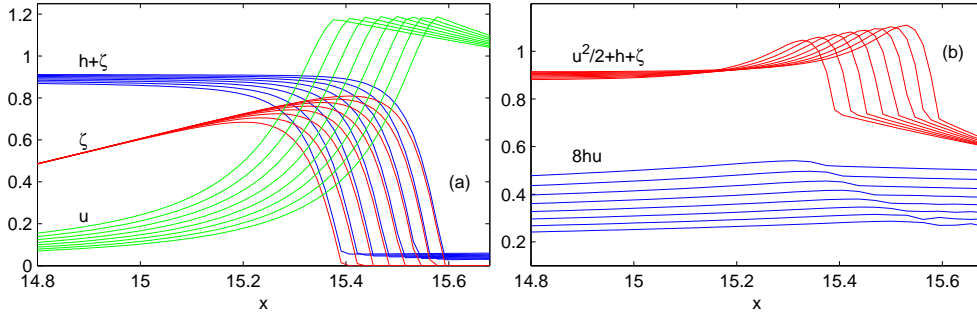


FIGURE 9. Snapshots of (a) $h + \zeta$, ζ and u and (b) $8q = 8hu$ and $\mathcal{B} = u^2/2 + h + \zeta$ during the runaway incision of the dam break computation shown in figure 8 (the snapshots are 0.8 time units apart).

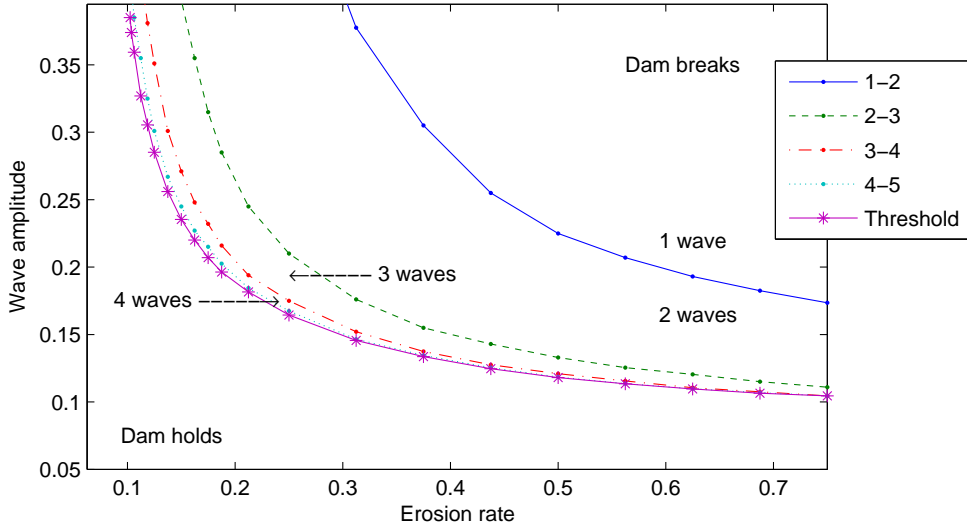


FIGURE 10. The threshold for the dam break on the (ϵ, A_0) -plane. Also indicated are the divisions between regions in which different numbers of waves are required to break the dam. The remaining parameter settings are as in figure 8.

of the initial disturbance and dam profile. This is illustrated in figure 11, which initializes the computation using the eigenfunction of the linear seiche, rather than equation (3.13), and reports other results regarding the timescales involved in the dam break. More specifically, figure 11 shows the total time taken to remove the dam, and the time taken for the runaway incision, t_I . To compute these times, we define the incision to begin when $\text{Max}(\zeta) = \zeta_m = 0.8$ (which provides a convenient and unambiguous, if somewhat arbitrary criterion) and end when $\text{Max}(\zeta) = \zeta_m$ first becomes equal to zero. This gives the time taken for the initial seiche, t_S , and the incision time, t_I ; the total time taken to remove the dam is then $t_S + t_I$.

Note that because the model does not incorporate deposition, only erosion, the downstream face of the dam is eroded first, which is where the water speed reaches its highest values, and this cuts away and steepens the right-hand flank. This feature is unphysical in the initial phases of the dam break during which the overtopping waves decelerate due to drag once they reach the flat plane beyond the dam. At this stage, the eroded material

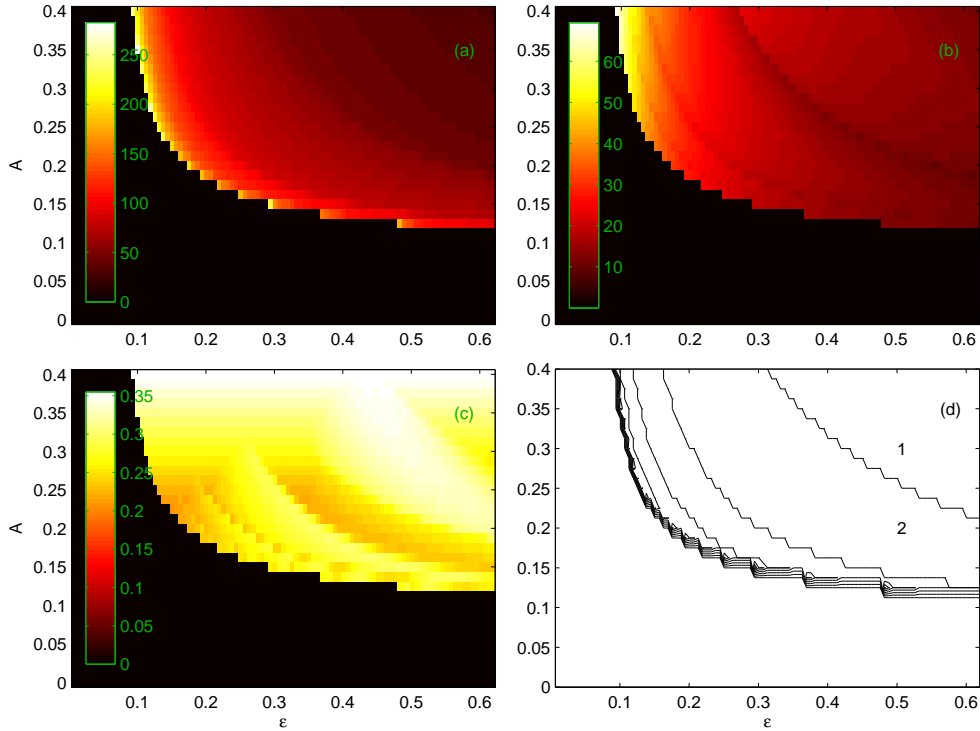


FIGURE 11. Details of dam breaks for the initial condition, $h(x, 0) = h_{eq}(x) + A_0 \cos(\pi x/\ell)$. The remaining parameter settings are as in figure 8. Panel (a) shows the total time required to remove the dam, and (b) shows the runaway incision time, t_I , both as densities on the (ϵ, A) -plane. Panel (c) shows the maximum value of the flux, $q = hu$, achieved during the computation, and (d) shows the borders between the regions in which varying numbers of waves were required to break the dam (*cf.* figure 10, for a different initial condition). In panels (a)-(c), the zero density level corresponds to no dam break.

should sediment from the relatively sluggish flow, leaving a skirt of deposition. Another consequence of including deposition is the eventual arrest of erosion and the formation of a wedge-shaped relic of the original dam (see section 2), whereas without deposition the whole dam is removed.

4. A simpler model

In most situations, the rate of erosion is relatively slow, $\epsilon \ll 1$. Thus, as fluid rushes over the dam on the hydrodynamic timescale, $\Delta/\sqrt{gZ_0}$, the bed remains largely in place; it is only eroded over a longer timescale. Similarly, when the reservoir is much longer than the dam ($\ell \gg 1$) and empties through a shallow breach, the seiche period and drainage time also greatly exceed $\Delta/\sqrt{gZ_0}$. Hence, the problem decomposes into two parts: in the reservoir, the slow, large-scale seiche is superposed on a gradually changing mean level. The reservoir feeds water towards the dam, where the outflow steadily adjusts to the slowly varying upstream head and gradually erodes that obstruction. The mathematical statement of these ideas leads to a simpler model of the dam break which is described below.

4.1. Dam hydraulics

In the vicinity of the dam, we ignore fast hydrodynamic adjustments by neglecting the time derivatives, h_t and u_t , in comparison to $(hu)_x$ and uu_x . We also drop the dissipative terms, $(c_f|u| + \lambda)u/h$ and νu_{xx} , which brake the eroding outflow over the dam. Although the experiments suggest that drag is quantitatively important (see section 2), neglecting it does not introduce a qualitative error (Pratt 1986 and Hogg & Hughes 2007). This reduces the system of equations (3.6)-(3.8) to

$$(hu)_x = \left(\frac{1}{2}u^2 + h + \zeta \right)_x = 0, \quad (4.1)$$

$$\zeta_t = -\epsilon E(u^2). \quad (4.2)$$

Equations (4.1) are familiar in hydraulics and imply that the water flux, q , and Bernoulli potential, \mathcal{B} , are constant in space:

$$q(t) = hu, \quad \mathcal{B}(t) = \frac{1}{2}u^2 + h + \zeta. \quad (4.3)$$

Equations (4.1) can also be written as the differential equation,

$$(u - q/u^2)u_x = -\zeta_x. \quad (4.4)$$

Regular solutions of equation (4.4) cannot be found at the singular point where $q = u^3$, unless we demand that $\zeta_x = 0$ at the same location. If $\zeta(x_m) = \zeta_m$, $u(x_m) = u_m$ and $h(x_m) = h_m$ at the maximum, $x = x_m$, then this requirement indicates that

$$q = u_m^3, \quad h_m = u_m^2 \quad \text{and} \quad \mathcal{B} = \frac{3}{2}q^{2/3} + \zeta_m. \quad (4.5)$$

Sufficiently far upstream of the dam, $\zeta \rightarrow 0$ and the water level approaches that of the reservoir, denoted h_L . Hence, using equation (4.3) $\mathcal{B} = h_L + q^2/(2h_L^2)$, and we arrive at an algebraic problem determining the flow conditions at the maximum of the dam:

$$\begin{aligned} 3q^{2/3} - q^2 h_L^{-2} &= 2(h_L - \zeta_m), & \text{if } h_L > \zeta_m, \\ q = u_m = h_m &= 0, & \text{if } h_L < \zeta_m. \end{aligned} \quad (4.6)$$

The second line of (4.6) applies when the water level is lower than the top of the dam and there is no outflow. The flow in the vicinity of the dam is therefore determined completely by the difference between the upstream water level and the dam maximum. In other words, the dam maximum ‘‘hydraulically controls’’ the water flux and evolves according to

$$\left(\frac{\partial \zeta}{\partial t} \right)_{x=x_m(t)} \equiv \frac{d\zeta_m}{dt} = -\epsilon E(u_m^2). \quad (4.7)$$

4.2. The lake dynamics

In the reservoir, $\zeta \rightarrow 0$, the shallow-water system reduces to equations (3.6) and (3.7), and we now retain the time derivatives because both the seiche and drainage are relatively slow. Let

$$\langle \dots \rangle \equiv \frac{1}{\ell} \int_0^\ell (\dots) dx \quad (4.8)$$

denote the spatial average over the reservoir. Then the mean water depth is $H = \langle h \rangle$, and (from integrating (3.6) and applying the boundary conditions at $x = 0$) satisfies

$$\frac{dH}{dt} = -\frac{q}{\ell}, \quad (4.9)$$

where q is the water flux through the dam region, as given by (4.6).

A crude model for the seiche dynamics can be extracted using a Galerkin-style approximation based on the gravest linear mode: We set $h = H(t) + \eta(x, t)$, and average (3.6) $\times \cos(\pi x/\ell)$ and (3.7) $\times \sin(\pi x/\ell)$ over the reservoir. After a little manipulation,

$$\frac{d}{dt} \langle \eta \cos(\pi x/\ell) \rangle + \frac{\pi H}{\ell} \langle u \sin(\pi x/\ell) \rangle = \frac{1}{\ell} [(H + \eta)u]_{x=\ell} - \frac{\pi}{\ell} \langle \eta u \sin(\pi x/\ell) \rangle \quad (4.10)$$

and

$$\frac{d}{dt} \langle u \sin(\pi x/\ell) \rangle - \frac{\pi}{\ell} \langle \eta \cos(\pi x/\ell) \rangle = \langle [\nu u_{xx} - (H + \eta)^{-1}(\lambda + c_f |u|)u - uu_x] \sin(\pi x/\ell) \rangle. \quad (4.11)$$

The first term on the right of (4.10) represents an outgoing flux due to wave transmission across the dam. It is possible to make estimates of this term but we neglect it here in the interest of simplicity. Finally, we take $\eta \ll H$ and compute the averages using the approximations

$$\eta \approx a(t) \cos(\pi x/\ell) \quad \& \quad u \approx b(t) \sin(\pi x/\ell), \quad (4.12)$$

to arrive at coupled pair of equations for the modal amplitudes, $a(t)$ and $b(t)$, which are quoted below.

4.3. The model

The equations of the simplified model consist of (4.6), (4.7) and (4.9) supplemented by the equations satisfied by the modal amplitudes, $a(t)$ and $b(t)$:

$$\frac{dH}{dt} = -\frac{u_m^3}{\ell}, \quad \frac{d\zeta_m}{dt} = -\epsilon(u_m^2 - u_*^2)_+^\alpha, \quad (4.13)$$

$$\frac{da}{dt} + \frac{\pi H}{\ell} b = 0, \quad \frac{db}{dt} - \frac{\pi}{\ell} a = -\left(\frac{\pi^2 \nu}{\ell^2} + \frac{\lambda}{H} + \frac{8c_f}{3\pi H} |b| \right) b, \quad (4.14)$$

where (because $h_L \rightarrow H - a$ for $x \rightarrow \ell$)

$$u_m^2 = \frac{2}{3}(H - a - \zeta_m)_+ + \frac{u_m^6}{3(H - a)^2}, \quad (4.15)$$

and the $+$ subscript on a variable X_+ is short-hand for $\text{Max}(X, 0)$, which conveniently incorporates the switching on and off of erosion and the flow over the dam. Note that equation (4.15) has multiple possible solutions in u_m , but only that solution for which $u_m = 0$ at $H - a - \zeta_m = 0$ is physically meaningful. Although the dambreak dynamics is now described by the four variables (H, ζ_m, a, b) , one must still solve (4.2) everywhere in order to compute the evolution of the full dam profile.

A sample solution is shown in figure 12 for an initial wave amplitude just above the threshold value required for dam break; the remaining parameter settings are the same as the numerical solutions of the full shallow-water equations displayed in figure 8. Although the reduced model qualitatively captures the dynamics of the full shallow-water system, the erosion is stronger in the reduced model, which can be attributed to the neglect of drag within the breach.

Thresholds on the (ϵ, A_0) plane (with $A_0 \equiv |a(0)|$) for the reduced model are shown in figure 13; the results qualitatively mirror those of figure 10. The figure also includes a conservative estimate of the threshold obtained by first making the approximation, $u_m^2 \approx (2/3)(H - a - \zeta_m)$, in (4.15), which is valid when $u^2 \ll h$ upstream of the dam. In

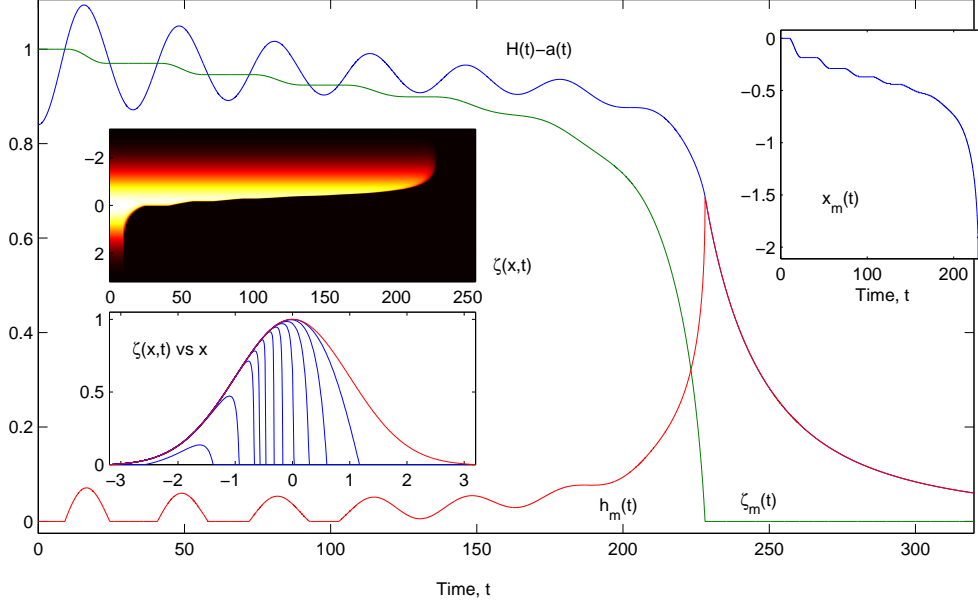


FIGURE 12. Solution of the reduced model, showing $H(t) - a(t)$, $\zeta_m(t)$ and $h_m(t)$ in the main picture, $x_m(t)$ in the inset on the right, and two insets of $\zeta(x, t)$ on the left (snapshots for $t = 0, 10, 13, 17, 37, 63, 114, 165, 191, 204, 219$ and 227 , and as a density on the (t, x) -plane, with shading increasing uniformly from 0 to 1). The initial amplitude is $a(0) = 0.124$ and the remaining parameter settings are as in figure 8.

this case, combining the equations in (4.13) gives

$$\frac{d}{dt}(H - \zeta_m) \approx \epsilon \left[\frac{2}{3} \left(H - a - \zeta_m - \frac{3}{2} u_*^2 \right)_+ \right]^\alpha - \frac{1}{\ell} \left[\frac{2}{3} (H - a - \zeta_m)_+ \right]^{3/2}. \quad (4.16)$$

The right-hand side of (4.16) expresses the competition between erosion of the dam and drainage of the reservoir, as modulated by the seiche, and must be positive in order for a breach to occur. Moreover, since the maximum of $H - a$ over the period of the seiche is invariably less than $h_0 + A_0$, and decreases faster than ζ_m when the dam does not break, we estimate the threshold by demanding that the right-hand side of (4.16) be positive for initial conditions with $H - a - \zeta_m = h_0 + A_0 - 1$, implying (on taking $\alpha = 3/2$)

$$\epsilon > \frac{(h_0 + A_0 - 1)_+^{3/2}}{\ell (h_0 + A_0 - 1 - 3u_*^2/2)_+^{3/2}}. \quad (4.17)$$

Figure 13 also shows the threshold for different choices of the parameters governing the damping of the seiche. The viscous parameter, ν , and Chézy coefficient, c_f , play a minor role unless given much larger values than the “standard” settings used in previous examples; the linear drag affects the threshold the most (at least when the dissipative terms only damp the seiche and do not brake the flow over the dam), and raises the actual condition above the estimate in (4.17).

Some other properties of the dam break are shown in figure 14. This figure shows the dambreak time, the runaway incision time t_I , the maximum value of the flux, $q = hu$, achieved over the dam break, and the number of waves needed to break the dam. This figure complements those shown earlier (figures 10 and 11) for the shallow-water model.

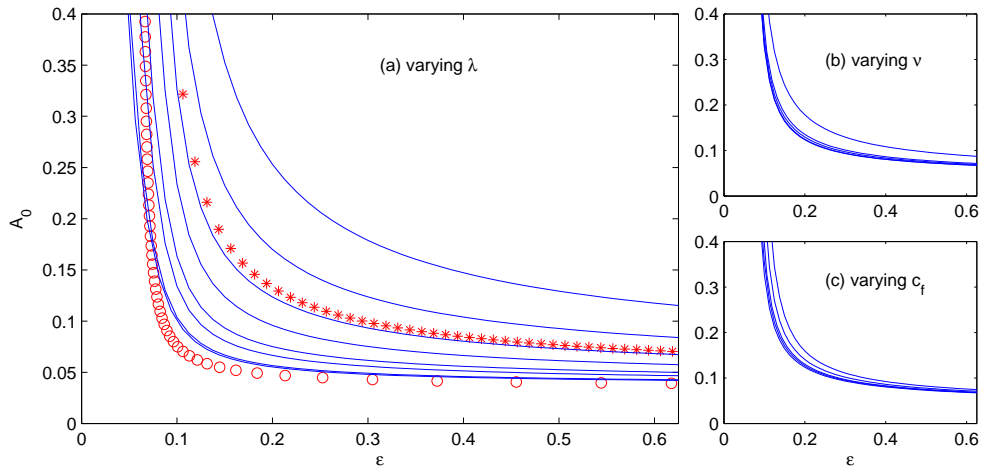


FIGURE 13. Dambreak thresholds for the reduced model. Panel (a) shows thresholds for different values of the drag parameter λ (the curves are for $\lambda = 0, 10^{-4}, 0.001, 0.002, 0.005, 0.01, 0.02$ and 0.04), with $c_f = 0, \nu = 0$. The stars show the threshold for the “standard” parameter settings of figure 8. The circles and crosses show the analytical prediction in (4.17). The other panels show the thresholds for $\lambda = 0.0125$ and (b) $\nu = 0, 0.008, 0.04, 0.08$ and 0.4 with $c_f = 0$, and (c) $c_f = 0, 0.0125, 0.025, 0.0625$ and 0.125 with $\nu = 0$. In all three panels, the smallest values of λ, ν and c_f correspond to the lowest of the curves, and the largest parameter setting to the highest curves. The other parameters are chosen as usual.

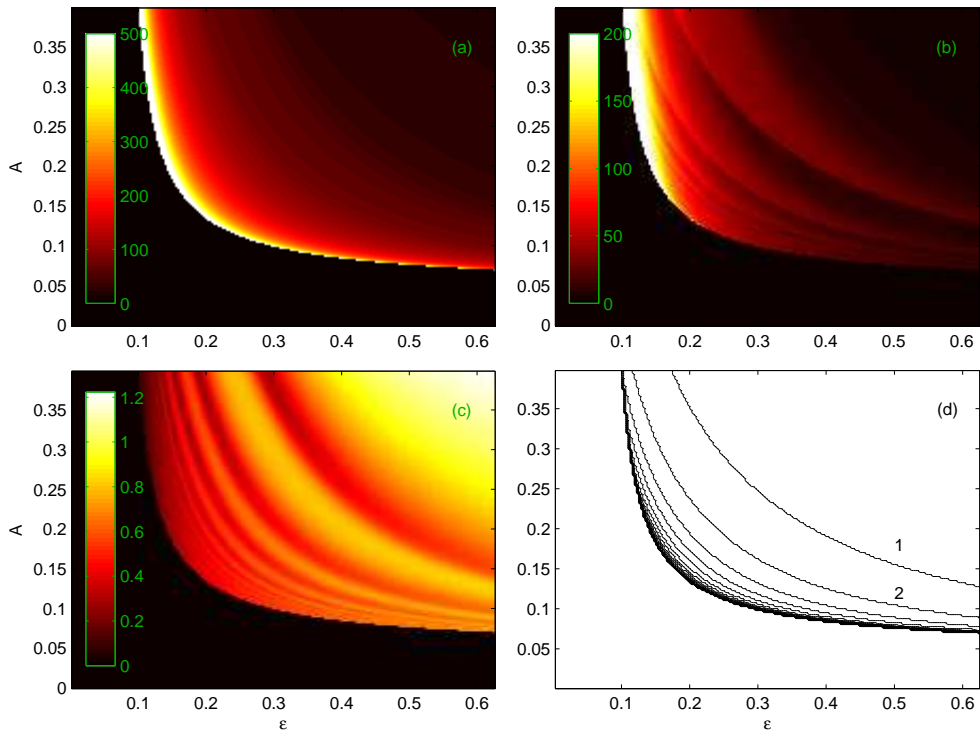


FIGURE 14. A figure equivalent to figure 11, but computed with the reduced model. Here, $A_0 \equiv a(0)$, and the remaining parameter settings are as in figure 8.

4.4. The incision

Once the runaway incision begins, the seiche largely damps away, $(a, b) \rightarrow 0$, so equations (4.13) and (4.15) simplify to

$$\frac{dH}{dt} = -\frac{u_m^3}{\ell}, \quad \frac{d\zeta_m}{dt} = -\epsilon(u_m^2 - u_*^2)_+, \quad u_m^2 = \frac{2}{3}(H - \zeta_m)_+ + \frac{u_m^6}{3H^2}, \quad (4.18)$$

which also offers a model for dam breaks initiated by overfilling the reservoir. By simplifying (4.18) still further, and assuming $\alpha = 3/2$, we may extract some estimates of the incision time and maximum flux: Assuming that $u_m \approx \sqrt{2(H - \zeta_m)/3} \gg u_*$, we may integrate (4.18) from the beginning of the incision, $t = t_S$ (*i.e.* the time for the initial seiche) when $\zeta_m = \zeta_I$ (chosen above to be 0.8) and $H = H_I$, up to its end, $t = t_S + t_I$ when $\zeta_m \rightarrow 0$. This gives a duration,

$$t_I \sim \frac{C}{\epsilon} [1 - (\epsilon\ell)^{-1}]^{-1}, \quad (4.19)$$

with

$$C = 2 \left(\frac{3}{2}\right)^{3/2} \left\{ (H_I - \zeta_I)^{-1/2} - \left[H_I - \frac{\zeta_I}{\epsilon\ell} \right]^{-1/2} \right\}. \quad (4.20)$$

If the mean lake level has yet to decline appreciably at the beginning of the incision, $H_I \approx 1$, completing the estimate of C . A yet cruder approximation is to assume that $H_I - \zeta_I \ll 1$, giving C the constant value of $2(3/2)^{3/2}(H_I - \zeta_I)^{-1/2} \approx 8$ (which leads to $t_I \approx 40$ for the dambreak of figure 12).

In both the shallow-water and reduced models, the maximum discharge, q_{max} (the greatest value of $|dH/dt|$), occurs at the end of the incision, when $t = t_S + t_I$ (*cf.* figure 12). At this instant, our approximation and integration of (4.18) implies

$$q_{max} = \frac{2}{3} \left[1 - \frac{\zeta_I}{\epsilon\ell} \right]^{3/2} \sim [1 - (\epsilon\ell)^{-1}]^{3/2}. \quad (4.21)$$

The predictions of the drainage time and maximum discharge in equations (4.19) and (4.21) are plotted as functions of ϵ in figure 15, where they are compared with data for the full shallow-water and reduced models (as extracted from figures 11 and 14). Note that there is no dependence in the predictions for t_I and q_{max} on the initial wave amplitude, A . Also the maximum flux in the shallow-water model can be achieved in the reservoir during the seiches (leading to the relatively flat values of q_{max} as functions of ϵ), a feature not captured by the reduced model.

After the incision has ceased, the lake drains away according to

$$H(t) = \left[H(t_S + t_I)^{-1/2} + \frac{(t - t_S - t_I)}{2\ell} \right]^{-2}, \quad (4.22)$$

which suggests a characteristic drainage timescale, $t_D \sim D\ell$, with D a factor of order unity. Defining, somewhat arbitrarily, that the dambreak has largely ended when $H = 0.1$, we find $D \approx 5$ (given $H(t_S + t_I) \approx 1$), which gives about 80 time units for the dambreak in figure 12.

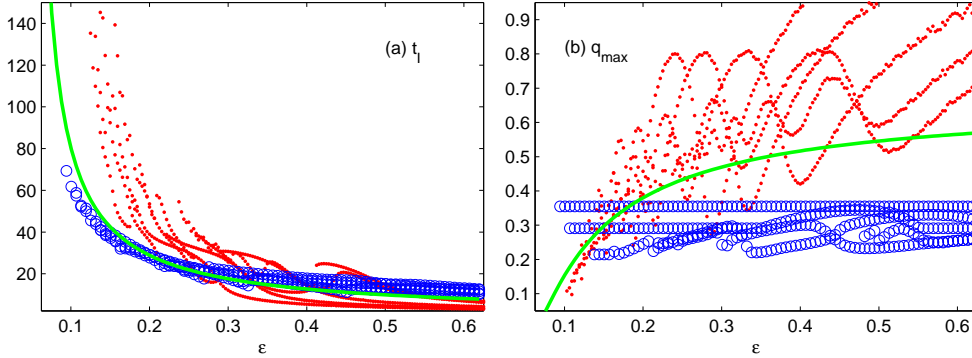


FIGURE 15. A comparison of (a) time for runaway incision (the time between the instants that $\zeta_m = 0.8$ and the dam is removed), and (b) maximum flux, $q = hu$, for the shallow-water model (circles), the reduced model (dots), and the estimates in (4.19) and (4.21) (solid lines). The data plotted correspond to the values of A of 0.4, 0.32, 0.25, 0.18 and 0.12.

5. Discussion

5.1. Dimensional considerations

The most important dimensionless groups of the theory are the combinations,

$$A, \quad \epsilon \equiv Wg\Delta, \quad u_* = \frac{U_*}{\sqrt{gZ_0}}, \quad \lambda \equiv \frac{\Lambda\Delta}{Z_0\sqrt{gZ_0}}, \quad r = \frac{1}{\epsilon\ell} = \frac{1}{WgL}, \quad d = 1 - \frac{H_0}{Z_0},$$

which, respectively, control the initial wave amplitude, the rate of erosion, the erosion threshold, the fluid drag, the rate of lake drainage compared to erosion ($L = \Delta\ell$ is the dimensional lake length), and the initial difference between the mean lake level (H_0) and the dam height (Z_0). The parameters all play an important role in the initial seiche phase, and hence the threshold for dam break: A , λ , r and d determine the degree and persistence of overtopping, whilst ϵ and u_* set the amount of erosion. Dimensional analysis demands that the threshold may formally be written as the condition, $A > A_c(\epsilon, u_*, \lambda, r, d)$, and the results presented in sections 3 and 4 offer some insight into the function A_c . Our crudest estimate suggests

$$A_c = d + \frac{2u_*^2}{3(1-r^{2/3})} \equiv \frac{Z_0 - H_0}{Z_0} + \frac{2U_*^2}{3gZ_0} \left(1 - \frac{1}{(WgL)^{2/3}}\right)^{-1} \quad (5.1)$$

(*cf.* equation (4.17)). The physical interpretation is that the initial wave height should exceed the difference between the lake level and dam height by an amount given by the need to surpass the erosion threshold, and weighted by a factor which ensures that the erosion rate overtakes the competing effect of lake drainage ($WgL > 1$).

Likewise, the total time for the reservoir to empty is formally given by a function, $t_B(A, \epsilon, \lambda, r, d, u_*)\Delta/\sqrt{gZ_0}$. The dimensionless timescale, t_B , can be split into three components, $t_B = t_S + t_I + t_D$, where t_S is the time of the initial seiche, t_I is the time for the runaway incision to occur once initiated, and t_D is the final drainage time after the erosion of the dam has been arrested. Once the seiche initiates the runaway incision, the details of the initial lake and wave disturbance become secondary. Hence, we may write

$$t_B = t_S(A, \epsilon, \lambda, r, d, u_*) + t_I(\epsilon, r, u_*) + t_D(\epsilon, r), \quad (5.2)$$

where our crudest estimates suggest that

$$t_I \sim \frac{C}{\epsilon(1-r)} \quad \text{and} \quad t_D \sim \frac{D}{\epsilon r}, \quad (5.3)$$

with numerical constants, $C \approx 8$ and $D \approx 5$.

Given the incision and drainage times, we estimate the characteristic discharge occurring in the dam break (the total fluid discharged divided by the duration of the dambreak, $t_I + t_D$, ignoring the initial seiche):

$$Q \sim \frac{H_0 L \sqrt{g Z_0}}{(t_I + t_D) \Delta}. \quad (5.4)$$

Peak discharges, on the other hand, can be as high as

$$Q_{max} \sim Z_0 \sqrt{g Z_0} q_{max}(A, \epsilon, u_*, \lambda, r, d), \quad (5.5)$$

where q_{max} is order one (*cf.* figures 11, 14 and 15). Our crude estimates suggest (*cf.* also equation (4.21)):

$$Q \sim \left(\frac{W g L - 1}{3 + 5 W g L} \right) H_0 \sqrt{g Z_0} \quad \text{and} \quad Q_{max} \sim Z_0 \sqrt{g Z_0} \left(1 - \frac{1}{W g L} \right)^{3/2}. \quad (5.6)$$

5.2. Comparing theory and experiment

To compare theory and the experiments, one must first match the empirical constants with the experiments. Neglecting deposition at the crest of the dam, our theoretical model of erosion takes the form, $d\zeta_m/dt = -W E(u_m)$. Consequently, by monitoring the dam height and water speed, one can measure the erosion parameter, W , once the threshold, U_* , in $E(u)$ is known. For sediment with a single particle size, that threshold can be expressed empirically as a Shields stress (Parker 2006),

$$\tau_* \equiv \frac{U_*^2}{R g D} \approx 0.5 \left[0.22 Re_p^{-0.6} + 0.06 \times 10^{-7.7 Re_p^{-0.6}} \right], \quad (5.7)$$

where

$$R = \frac{\rho_s - \rho}{\rho}, \quad Re_p = \frac{(R g \delta)^{1/2} \delta}{\nu}, \quad (5.8)$$

are the excess density and particle Reynolds number respectively, and ρ_s and δ are the particle density and mean diameter (ρ is the fluid density and ν is the fluid kinematic viscosity). Proceeding down this route for the coarse sand, we arrive at the estimates, $Re_p \approx 100$ and $U_* \approx 0.015$ m/sec.† This threshold speed is much less than the observed flow speeds over the dam's crest (see figure 5), and so $W \approx u_m^{-3} (d\zeta/dt)$ (using $\alpha = 3/2$). Thence, $W \approx 0.26 \pm 0.1$ sec²/m² for the data from the narrow tank, and $W \approx 0.15 \pm 0.1$ sec²/m² from the wide tank, which are consistent and suggest we adopt the nominal value, $W = 0.2$ sec²/m². The erosion parameter, W , and threshold, U_* , then translate to the estimates, $\epsilon = g W \Delta \approx 0.2$ and $u_*^2 = U_*^2 / (g Z_0) \approx 10^{-4}$ (with $Z_0 \approx 0.1$ m and $\Delta \approx 0.1$ m).

The primary damping of the seiche in the experiments arises through viscous dissipation in Stokes' layers adjacent to the walls of the tank. The effective damping rate can

† An analogous calculation for the bimodal mixtures cannot be made since reliable formulae equivalent to (5.7) do not exist for such materials.

be estimated to be of order,

$$\Lambda \approx \left(\frac{\pi^2 \nu^2 g}{4L^2 H_0^3} \right)^{1/4} \sim 0.01 \text{ sec}^{-1}.$$

Hence, $\lambda = \Lambda \Delta / Z_0 \sqrt{gZ_0} \sim 0.01$. Given that $\Delta / Z_0 \sim 1$, the estimates of C_f , which range from 0.1 for rough walls to 0.001 for smooth ones, translate to equivalent values of the dimensionless drag parameter, c_f . Finally, the viscous coefficient, ν , would be of order 10^{-5} if the molecular value of viscosity were appropriate, but could be as large as 10^{-2} if this quantity parameterized turbulent eddies with characteristic speeds of 0.1 m/sec and lengthscales of 0.01 m (suggesting an effective kinematic viscosity of $10^{-3} \text{ m}^2/\text{sec}$).

Given these “experimental” parameter settings, we may now briefly compare the observations and theory: for A_c , the theoretical models suggest that the threshold in initial wave amplitude should be about 15 percent of the water depth. This prediction is close to the observation reported in section 2 that the critical value was around ten percent. Crude estimates of the experimental dam break time and maximum flux can be extracted from the time series of lake level shown in figure 6, and are order 20 or 30 seconds and $2.4 \times 10^{-3} \text{ m}^2/\text{sec}$, respectively ($q \approx -LdH/dt$). Direct measurements of the flux within the breach using tracer particles are rather higher ($4 \times 10^{-3} \text{ m}^2/\text{sec}$ or more, see figure 5). Theory predicts a dimensionless time for incision and drainage of order a hundred. Coupled with the characteristic timescale, $\Delta / \sqrt{gZ_0} \sim 0.1 \text{ sec}$, used in the non-dimensionalization, this corresponds to a time of 10 seconds. The corresponding maximum flux from (5.6) is $3.5 \times 10^{-2} \text{ m}^2/\text{sec}$. Notice that these theoretical predictions are sensitive to the material properties and in particular on the estimate of $r = 1/(WgL)$. Further, the difference in theoretical estimates may be due to deposition, which plays a key role in arresting erosion in the later stages of the experimental dam breaks, an effect not fully accounted for in the current theory. Alternatively, we have also ignored the feedback of the sediment on the flow dynamics, and in particular the eroded mass added to the flow, which could reduce the flux and lengthen the duration of the dambreak.

6. Conclusions

In this article, we have modelled, both experimentally and theoretically, how a dam can be broken by a combination of overtopping waves and runaway erosional incision. The experiments demonstrate the feasibility of the scenario, and the phenomenology can be qualitatively reproduced by theoretical models. The ingredients of those models include a slowly decaying seiche in the dammed reservoir that feeds water to a hydraulically controlled breach in the dam. Whether the model incorporates these ingredients within a shallow-water formulation, or in a simpler conceptual model capturing the main global variables (dam height, reservoir depth and seiche amplitude), the dam break process amounts to a competition between erosion, lake drainage and seiche damping. A threshold naturally results wherein the initial wave amplitude, or rate of erosion, should exceed a critical value for a break to occur.

A key limitation of our theoretical analysis is that it is two-dimensional, whereas moraine-dammed lakes are complicated three-dimensional structures. In fact, a puzzling observation in the experiments is that discharges are comparable in both narrow (5 cm width) and wide (20 cm width) tanks (see figure 6), and the width of the incised channels in the latter appears unimportant. Theoretical computations with the three-dimensional generalization of the shallow-water model (Balmforth *et al.* 2008) also suggest that discharges, and even the erosion threshold, are weakly sensitive to the third dimension.

This result can be rationalized by the fact that, for steady flow in a three-dimensional channel of slowly varying width, the concept of hydraulic control still applies, but to the cross-channel averaged flow speed and depth. The three-dimensional water flux is therefore given by $q^{3D} \sim b\bar{h}\bar{u} \rightarrow b\bar{u}_m^{3/2}$, where b is the channel's width and the overbar signifies a cross-channel average. The average speed, \bar{u}_m , is once more determined by the upstream head, $H - \zeta_m$, and we feed the resulting flux into the lake drainage equation, $dH/dt = -q^{3D}/\mathcal{A}$, where \mathcal{A} is the lake area. But $b/\mathcal{A} \rightarrow L^{-1}$ at the entrance of the channel, furnishing $dH/dt \sim -\bar{u}_m^{3/2}/\ell$ as in the two-dimensional problem considered here. In other words, the difference between the breadth of the lake and the width of the breach in the dam does not play a role, as might have originally been thought. More generally, one expects that ratio of lake breadth to breach width becomes important when the lake is much wider than the dam breach, and there is a sudden expansion in b at the entrance of the channel. In our experiments and shallow-water computations, the breach is only three or so times narrower than the lake width. In geological settings, the lake could be rather wider and the argument less compelling. Furthermore, other physical effects, such as the focussing of a displacement wave into a narrow pre-existing channel (Blown & Church 1985), might dominate the phenomena studied here.

We thank Antonello Provenzale for the negative remarks that helped to drive this work forward. The experiments were conducted at the Coastal Research Laboratory, Woods Hole Institute of Oceanography, during the 2006 Geophysical Fluid Dynamics Summer Study Program (which was supported by the National Science Foundation). We thank Keith Bradley for assistance with the experiments, and the participants at Walsh Cottage for discussions.

REFERENCES

- BALMFORTH, N. J., VON HARDENBERG, J., PROVENZALE, A. & ZAMMETT, R. 2008 Dam breaking by catastrophic erosional incision, *J. Geophys. Res.*, **113**, F01020, doi:10.1029/2007JF000756
- BLOWN, I. G. & CHURCH, M. 1985 Catastrophic lake drainage within the Homathko river basin, British Columbia, *Canadian Geotechnical Journal*, **22**, 551-553.
- BORIS, J. P. & BOOK, D. L. 1976 Solution of Continuity Equations by the Method of Flux-Corrected Transport, *Methods of Computational Physics* (Academic Press, New York), **16**, pp. 85-129.
- CAO, Z., PENDER, G., WALLIS, S. & CARLING, P. 2004 Computational dam-break hydraulics over erodible sediment bed, *J. Hydr. Eng. ASCE*, **130**, 689-703.
- CLAGUE, J.J. & EVANS S.G. 2000 A review of catastrophic drainage of moraine-dammed lakes in British Columbia, *Quat. Sci. Rev.*, **19**, pp. 1763-1783.
- CLARKE, G.K.C. 1987 Subglacial Till: A Physical Framework for Its Properties and Processes, *J. Geophys. Res.*, **92(B9)**, pp. 9023-9036.
- COLEMAN, S. E., ANDREWS, D. P. & WEBBY, M. G. 2002 Overtopping breaching of noncohesive homogeneous embankments, *J. Hydr. Eng. ASCE*, **128**, 829-838.
- COSTA, J. E. & SCHUSTER, R. L., 1988 The formation and failure of natural dams, *Bull. Geol. Soc. America*, **100**, pp. 1054-1068.
- HOGG, A. M. & HUGHES, G. O. Shear flow and viscosity in single-layer hydraulics, *J. Fluid Mech.*, **548**, pp. 431-443.
- HUBBARD, B., HEALD, A., REYNOLDS, J. M., QUINCEY, D., RICHARDSON, S. D., LUYO, M. Z., PORTILLA, N. S. & HAMBREY M. J. 2005 Impact of a rock avalanche on a moraine-dammed proglacial lake: Laguna Safuna Alta, Cordillera Blanca, Peru, *Earth Surface Processes and Landforms*, **30**, pp. 1251-1264.
- KERSHAW, J. A., CLAGUE, J. J. & EVANS, S. G. 2005 Geomorphic and sedimentological sig-

- nature of a two-phase outburst flood from moraine-dammed Queen Bess Lake, British Columbia, Canada, *Earth Surface Processes and Landforms*, **30**, DOI: 10.1002/esp.1122.
- KEULEGAN, G. H. 1959 Energy dissipation in standing waves in rectangular basins, *J. Fluid Mech.*, **6**, 33-50.
- McKILLOP, R. J., & CLAGUE, J. J. 2006 A procedure for making objective preliminary assessments of outburst flood hazard from moraine-dammed lakes in southwestern British Columbia, *Natural Hazards*, **30**, DOI: 10.1007/s11069-006-9028-7.
- McKILLOP, R. J., & CLAGUE, J. J. 2007 Statistical, remote-sensing based approach for estimating the probability of catastrophic drainage from moraine-dammed lakes in southwestern British Columbia, *Global & Planetary Change*, **56**, 153-171.
- PARKER G. 2006 1D sediment transport morphodynamics with applications to rivers and turbidity currents, http://cee.uiuc.edu/people/parkerg/morphodynamics_e-book.htm (last updated April 13 2006),
- PRATT, L. J. 1986 Hydraulic Control of Sill Flow with Bottom Friction, *J. Phys. Oceanogr.*, **16**, pp. 1970-1980.
- RABASSA J. RUBULIS S. AND SUAREZ J. 1979 Rate of formation and sedimentology of (1976-1978) push-moraines, Frias Glacier, Mount Tronadoz ($41^{\circ}10'$ S; $71^{\circ}53'$ W), Argentina, in Schluchter C. (ed.): *Moraines and varves: origins, genesis, classification* (Rotterdam, Balkema).
- TAKI K. AND PARKER G. 2004 Transportational cyclic steps created by flow over an erodible bed. Part 1. Experiments, *J. Hydraulic Res.*, **43(5)**, pp. 488-501.
- TAKI K. AND PARKER G. 2004 Transportational cyclic steps created by flow over an erodible bed. Part 2. Theory and numerical simulation, *J. Hydraulic Res.*, **43(5)**, pp. 502-514.
- ZALESK, S. T. 1979 Fully Multidimensional Flux-Corrected Transport, *J. Comp. Phys.* **31**, 335-362.